Received: 13 April 2021 | Revised: 16 June 2021 | Accepted: 22 June 2021

DOI: 10.1002/pro.4151

FULL-LENGTH PAPER

THE PROTEIN SOCIETY WILEY

Cryptic association of B7-2 molecules and its implication for clustering

Swetha Lankipalli[1,2] | **Mahadeva Swamy H S**[3] | **Deepak Selvam**[4,5] | **Dibyendu Samanta**[6] | **Deepak Nair**[3] | **Udupi A. Ramagopal**[1]

[1]Biological Sciences Division, Poornaprajna Institute of Scientific Research (PPISR), Bengaluru, India

[2]Manipal Academy of Higher Education, Manipal, Karnataka, India

[3]Centre for Neuroscience, Indian Institute of Science, Bangalore, India

[4]Jawaharlal Nehru Center for Advance Scientific Research, Bengaluru, Karnataka, India

[5]National Institute for Research in Tuberculosis, Chennai, India

[6]School of Bioscience, Sir J. C. Bose Laboratory Complex, Indian Institute of Technology Kharagpur, Kharagpur, India

Correspondence
Udupi A. Ramagopal, Biological Sciences Division, Poornaprajna Institute of Scientific Research (PPISR), Bidalur post, Devanahalli, Bengaluru, 562164, India.
Email: ramagopal.udupi@gmail.com

Funding information
IISC-STARs program grant, Grant/Award Number: PID 563; Vision Group on Science and Technology (VGST), Grant/Award Number: #191

Abstract

T-cell co-stimulation through CD28/CTLA4:B7-1/B7-2 axis is one of the extensively studied pathways that resulted in the discovery of several FDA-approved drugs for autoimmunity and cancer. However, many aspects of the signaling mechanism remain elusive, including oligomeric association and clustering of B7-2 on the cell surface. Here, we describe the structure of the IgV domain of B7-2 and its cryptic association into 1D arrays that appear to represent the pre-signaling state of B7-2 on the cell membrane. Super-resolution microscopy experiments on heterologous cells expressing B7-2 and B7-1 suggest, B7-2 form relatively elongated and larger clusters compared to B7-1. The sequence and structural comparison of other B7 family members, B7-1:CTLA4 and B7-2:CTLA-4 complex structures, support our view that the observed B7-2 1D zipper array is physiologically important. This observed 1D zipper-like array also provides an explanation for its clustering, and upright orientation on the cell surface, and avoidance of spurious signaling.

KEYWORDS

B7-2 structure, immune checkpoint blockade, immune receptors, protein clustering

1 | INTRODUCTION

B7-2 (CD86) is a type-1 transmembrane glycoprotein that belongs to the immunoglobulin superfamily (IgSF) and is expressed constitutively on antigen-presenting cells (APCs).[1] B7-2 and its close homologue B7-1 act as ligands for the co-stimulatory/inhibitory receptors CD28/CTLA-4 present on T-cells. According to the two-signal model of T-cell activation,[2,3] T-cells receive the first signal, which is antigen-specific, when the T-cell receptor (TCR) interacts with the antigenic peptide-loaded MHC (pMHC) present on the APC. The second co-signal, which is nonspecific, is provided by either co-stimulatory or co-inhibitory molecules that promote activation or suppression of the T-cell, respectively. The co-signal is provided by the interaction of co-stimulatory/inhibitory receptors of the CD28 family on the T-cell (CD28, CTLA-4, ICOS, PD-1, etc.) with their cognate ligands that belong to the B7 family present on APC.[4] These co-signaling molecules and clusters of adhesion molecules are shown to encircle the TCR-pMHC complex and form an immunological synapse (IS) between the T-cell and APC leading to a significant event in T-cell activation.[5–7] CD28/CTLA-4:B7-1/B7-2 axis is one of the earliest discovered and most

studied pathways where the interaction of CD28 with B7s synergizes the T-cell activation,[8] in contrast, the interaction of CTLA-4 with B7s attenuates the same.[9] The opposing functions of CD28 and CTLA-4 have an important role in maintaining peripheral tolerance and in avoiding auto-immunity.[10] Although B7-1 and B7-2 appear to have redundant functions, the differences in their temporal expression, their affinities towards the partners, and their oligomerization potential have established them as nonredundant but functionally overlapping molecules.[11] B7-2 is shown to be expressed constitutively on APCs while B7-1 is induced following activation.[12] Likewise, among CD28 and CTLA-4, CD28 is shown to be constitutively expressed on the T-cells while CTLA-4 is induced after activation. The equilibrium disassociation constants (K_d) of B7-2 for CD28 and CTLA-4 are ~2.6 μM and ~ 20 μM, respectively, while the corresponding values for B7-1 are ~0.2 μM and 4 μM, respectively.[13] Thus, the binding affinity of B7-2 for CD28 and CTLA-4 are ~5 to ~10 fold lower compared with that of B7-1. Based on the differences in the expression patterns, binding affinities and other supporting data pertaining to these receptor-ligand partners, it has been proposed that B7-2 is the preferential partner for CD28 and B7-1 for CTLA-4.[14] The molecules of CD28 axis have been shown to be in close proximity to the TCR: MHC complex in the central supramolecular activation complex (cSMAC) region of the IS and play a central role in the regulation of T-cell activation.[15] Demonstrating the prominence of these receptor-ligand interactions, the manipulators of this pathway are proven to be effective therapeutics to combat autoimmunity (e.g., Abatacept, Belatacept-immunomodulatory drugs that block CD28-B7-1/B7-2 interaction)[16,17] as well as cancer (e.g., the first-in-class mAb called Ipilimumab, an immune checkpoint inhibitor that works by blocking CTLA-4:B7-1/B7-2 interaction).[18]

Apart from the much-established role of B7-2 as a signaling partner for CD28 and CTLA-4, recent studies suggest an important role of B7-2 in hepatitis C virus (HCV) entry, entry of adenovirus species, and the progression of HIV infection.[19–21] The immunomodulatory role of B7-2 along with other B7 family members in renal, breast, and pancreatic cancers has also been elucidated.[22–24] Hence, there is a need for a detailed understanding of this protein with respect to its structure and physiological organization on the cell surface to strategically design therapeutic molecules that are effective manipulators of B7-2 mediated pathways.

B7-2 shares a sequence identity of only 26% with its close homologue B7-1, yet both of them bind to CD28 and CTLA-4.[25] The domain organization of B7 molecules comprises a membrane distal IgV domain and a membrane-proximal IgC domain, that extends into an extracellular juxtamembrane linker (EJ-linker) followed by a single-pass transmembrane domain and an intracellular cytoplasmic domain (Figure S1A). The structure of B7-1 ectodomain comprising both IgV and IgC domains has been determined both in apo form and in complex with CTLA-4.[26,27] In contrast, the B7-2 structures reported so far (including the present study and the one in complex with CTLA-4) are only that of the IgV domain.[28,29] The IgV domain of B7-1/B7-2 harbor the binding site of their cognate partners and the IgC domain is proposed to stabilize the IgV domain and provide the required length to interact with their cognate partners at the IS. Both structural and biophysical studies have shown that B7-1 is a homodimer in its apo form as well as in complex with CTLA-4.[26,27] In contrast, the apo B7-2 was shown to be monomeric in solution and in the crystal structure,[29,30] whereas based on the crystal structure of B7-2:CTLA-4 complex, it was proposed that B7-2 forms a receptor-induced dimer.[28] The dimeric association of B7-2 as seen in B7-2:CTLA-4 complex structure is very similar to that observed for B7-1 dimer.[28] Further, the mode of association of B7-2 dimer with CTLA-4 dimer is similar to the association of B7-1 dimer with CTLA-4 dimer (Figure S2). In both the complexes, continuous and alternate arrangements of CTLA-4 dimer with B7-1 or B7-2 dimers observed in the crystal structures results in a one-dimensional array mimicking the co-stimulatory receptor-ligand interactions and clustering that is reminiscent of the immunological synapse proposed for this class of molecules. Although, B7-2 exist as a monomer in solution, it has also been shown that B7-2 exist as a cluster, both on the vesicle and on the surface of the cell membrane of dendritic cells by immunoelectron microscopy (IEM).[31] Further, CTLA-4 dimer binds to B7-2 on the surface of APC with high avidity, but with lesser avidity in solution. Based on this observation and together with other supporting data B7-2 has been proposed to exist as clusters or oligomerizes on the APC even prior to its interaction with CTLA-4.[32] Notably, since both B7-2 and its preferred partner CD28 are constitutively expressed,[14] the presence of B7-2 as a pre-existing cluster calls for a probable physiological significance. This kind of pre-existing cluster is important for the avoidance of spurious signaling in the case of Zap70[33] and probably might be true in the case of B7-2 too.

Numerous experimental observations largely support the view that the nanoclustering of cell surface proteins is a dominant organizing principle of the plasma membrane.[34] However, the physicochemical factors that govern the sorting of these macromolecules into specified clusters with little overlapping on the cell membrane is still a matter of debate. Popular models including the

"lipid-raft" model[35] and the "fence and pickets" model[36] fail to capture and emulate the mechanistic details of specific association of a diverse class of proteins on the cell surface. Indeed, among the many mysteries of the cell, how cell-surface receptors stand in an orientation favorable to interact with their cognate partner (which we call as "upright" orientation) is a question of interest. This question is more pertinent particularly to those proteins containing several extracellular domains (many IgSF family members, adhesion molecules like cadherins, etc.,) and with a single pass transmembrane helix traversing through flexible cell membrane. Unfortunately, the limitations of the existing biophysical and biochemical techniques make it extremely difficult to visualize the intricacies of the protein conformation and dynamics on the cell membrane.[37] Probably, transient and weak *cis* oligomerization or clustering of these molecules, at least in some cases, appears to provide the answer for the unsolved puzzle of how monomeric cell surface proteins stand in an "upright" orientation on the cell membrane. Such *cis* association has been proposed for some of the adhesion proteins and other proteins involved in immune signaling.[38–40] In particular, B7-2 being a monomer in solution, either *cis* oligomerization or clustering appear to support its "upright" orientation and effective function on the cell surface.

Here, we present a high-resolution crystal structure of the receptor-binding domain of human B7-2 solved at 1.9 Å with four molecules in the asymmetric unit (ASU). The structure revealed a preferred and physiologically relevant dimer-like orientation, where the C-terminal ends of the IgV domains of associating molecules are in proximity. Interestingly, the two dimers present in the ASU are similar to each other, which is unusual considering the possibility of repetition of an accidental dimer-like association being infinitesimally small. Crystal packing analysis suggests that each dimer in ASU is part of a two distinct supramolecular organization of 1D zipper-like array that runs through the crystal. The C-terminal end of all the molecules in the array face in one direction mimicking the situation required for clustering of these molecules on the cell surface. Our super-resolution microscopy experiments also indicate that B7-2 form clusters on the cell-surface. We believe, the crystal structure provides the first atomic-level description of clustering of B7-2, which is driven by shape complementarity together with polar interactions (velcro of weak interactions) that drive the ordered association of these molecules at higher concentrations. We are intrigued that the observed dimer-like association in our crystal structure probably represents a relic of transient weak oligomers on the APC that is formed to avoid spurious signaling events. Further, we validate our observations by comparing them with many other protein structures already reported and did a detailed bioinformatic analysis to define the possible reasons that might be contributing to the "upright" orientation of B7-2 on the cell surface.

2 | MATERIALS AND METHODS

2.1 | Cloning, expression, and purification of B7-2

The hB7-2 gene spanning the IgV domain (Uniport Id: P42081, amino acids 26–134) was cloned into pNIC28-Bsa-4 vector by ligation independent cloning.[41] The protein was overexpressed in BL21(DE3) competent cells by inducing with 1 mM IPTG at 37°C. The protein was insoluble and formed an inclusion body which was purified and refolded by fast dilution method as described in reference 30. The refolded protein was concentrated and buffer exchanged to 20 mM HEPES, pH = 7.2, 150 mM NaCl, 1 mM EDTA using Amicon stirred cell with 3KDa Molecular weight cut-off membrane and purified by FPLC on a superdex-75 size exclusion column.

2.2 | Crystallization of B7-2

The N-terminal 6xHis-tag was cleaved using Tobacco Etch Virus (TEV) protease and the protein was further concentrated to 3.9 mg/ml using Millipore 3KDMW cut-off concentrator. The concentrated protein was screened with an MCSG-2 crystallization screen from Microlytic, USA. The crystallization was set up using the sitting drop vapour diffusion method in 96-well Intelliplates (Art Robbins). Sitting drops with a 1:1 mixture of 0.8 μl each of the protein solution (3.9 mg/ml of protein in 20 mM HEPES, pH = 7.2, 150 mM NaCl, 1 mM EDTA) and reservoir solution were equilibrated against 50 μl of reservoir solution at room temperature. Crystals appeared in more than five conditions. However, most crystals appeared as an agglomeration of several crystals. Best crystals from the condition containing 100 mM Tris–HCl, 2.4 M Ammonium phosphate dibasic pH = 8.5 were flash-frozen in the mother liquor supplemented with 20% glycerol as cryoprotectant.

2.3 | Data collection and structure solution

Data sets were collected at the beamline MASSIF-3, European Synchrotron Radiation Facility (ESRF), Grenoble, France, at a wavelength of 0.968 Å, on a DECTRIS EIGER X 4M PIXEL detector and the best crystal

diffracted to 1.90 Å resolution. As mentioned above, even after several optimization trials, most crystals were looking like an agglomeration of multiple lattices and diffraction was consistent with such observation and required data collection on several crystals. One of those crystals diffracted to high-resolution and it was possible to index the lattice parameters. The data sets were integrated and scaled using the program HKL2000.[42] The diffraction was consistent with the space group $P2_1$. ($a = 32.90$, $b = 81.64$, $c = 73.49$, $\beta = 90.32°$, solvent content 35.94%).

The structure was determined using the molecular replacement program MOLREP with B7-2 IgV domain structure (PDB entry: 1NCN) as a model.[43] The structure was refined using REFMAC5, CCP4-suite.[44] Model building was carried out using the program COOT.[45] The model was improved further by iterative cycles of restrained refinement followed by model improvement with COOT. Final coordinates were refined with TLS refinement and validated before submission to Protein Data Bank (PDB entry: 5YXK). The details of the data collection and refinement statistics are given in Table 1.

TABLE 1 Data collection and refinement statistics for high resolution structure of hB7-2

PDB code	5YXK
Source	ESRF MASSIF-3
Wavelength (Å)	0.968
Resolution limits (Å)	36.74–1.90
Space group	P 1 2_1 1
Unit-cell parameters (Å)	$a = 32.90$, $b = 81.64$, $c = 73.49$, $\beta = 90.32°$
No. of observations	125,778
No. of unique reflections	30,622
Completeness (%)	98.7 (97.8)
Mean $I/\sigma(I)$	11.82(3)
R_{merge} on $I^{\pm}$	0.107(0.351)
R_{pim}	0.057(0.243)
$CC_{1/2}$	0.986 (0.780)
Redundancy average	4.1
Refinement statistics	
Resolution limits (Å)	36.74–1.90
No. of reflections	28,723
Protein/water atoms	3603/81
R_{work}	0.199
R_{free}	0.248
Ramachandran plot statistics %	97 (favoured), 3(allowed),0 (outlier)

Note: Values in parentheses indicate statistics for the high-resolution data bin for X-ray and refinement data.
$Rmerge = \sum hkl \sum i|I(hkl)i - <I(hkl)>| / \sum hkl \sum i < I(hkl)i>$.
$Rpim = \sum hkl \{1/[N(hkl)-1]\}1/2 \times \sum i|I(hkl)i - <I(hkl)>| / \sum hkl \sum i < I(hkl)i>$, where N is the redundancy.

2.4 | Sequence conservation analysis

For sequence conservation analysis, the human B7-2 sequence (Uniprot Id: P42081) was chosen as a query sequence and the BLAST search was done using the non-redundant database of NCBI-BLAST.[46] The residues 33–225 spanning the IgV and IgC domains of hB7-2 were used as a query sequence. The initial hits were further filtered by choosing a percent identity cut-off of minimum-50% and a maximum identity cut-off of 95% with a query coverage of 85%. The resultant hits were manually curated to further remove any close isoforms and a final list of 86 unique sequences of B7-2 from different organisms was generated. The sequences were aligned using the multiple sequence alignment program Clustal Omega.[47] For better visualization, colored sequence alignment images were generated using ESPript 3.0[48] and the sequence logos were generated using BlockLogo.[49] The sequence conservation analysis of human B7-1 (Uniprot ID: P33681) was done in a similar way with the residues 35–230 covering both IgV and IgC domains. For sequence conservation analysis of B7-family members, individual sequences of B7-family members were taken from uniport and aligned using Clustal Omega.

2.5 | Super-resolution microscopy experiment

Plasmid construction: The plasmid pEZ-M98 vector with B7-1:GFP gene was a generous gift from prof. Steven C. Almo, Albert Einstein College of Medicine, New York. To generate plasmid with B7-2:GFP fusion construct, B7-2 and monomeric GFP genes were fused with overlap PCR and the B7-2:GFP fusion construct was cloned into pEZ-M98 vector using the restriction enzymes BstbI and XhoI. Both B7-1 and B7-2 genes have monomeric GFP as a C-terminal fusion to their transmembrane domain that eventually places GFP in the cytosol and the B7-2/B7-1 proteins will be tethered to the membrane on the extracellular side. Monomeric GFP was chosen as the fluorescent marker to avoid the influence of dimeric GFP on the clustering of the proteins under study.

Mammalian cell culture and transfection: Neuroblastoma cells (Neuro-2a, ATCC CCL-131) were cultured in DMEM supplemented with Glutamax, 1% fetal bovine serum and 1% penicillin—streptomycin at 37°C. Cells were grown in a 5% CO_2 incubator as discussed previously.[50] The transient transfection of the foresaid with plasmids using Turbofect reagent (Thermo Fisher

Scientific) as described in the manufacturer's guidelines and consistent with previous reports.[50,51] The cells expressing B7-2:GFP and B7-1:GFP will be referred to as B7-2 and B7-1, respectively. Morphologically similar cells with comparable expression of B7-2 and B7-1 were chosen for microscopy.[50,51]

2.6 | Immunocytochemistry

Neuro2A cells transfected with the plasmids were fixed with 4% paraformaldehyde and 4% sucrose in PBS for 10 min at 4°C and incubated in 0.1 M glycine in PBS for 5 min at room temperature. Fixed cells were washed using 1XPBS. Cells were permeabilized with 0.25% TritonX-100 in PBS for 5 min and washed with 1X PBS. Cells were treated with the blocking solution (10%BSA in PBS) for 30 min at room temperature. Then, cells were incubated with the primary antibody in 3% BSA in PBS for 1 h in a humidified chamber and washed with 3% BSA in PBS. Next, the cells were counter labelled with secondary antibody in 3% BSA in PBS for 45 min in a humidified chamber and washed with IXPBS. Prior to dSTORM imaging, the immunolabeled cells were fixed in 2% paraformaldehyde and 2% sucrose in PBS for 10 min at 4°C and washed with 1XPBS. In the study, we have used rabbit anti-GFP antibody (Thermofisher A-11122) with the dilution of 1:1000 and anti-rabbit Alexa fluor-647 dye with the dilution of 1:500 (Invitrogen, A-21245).

2.7 | dSTORM imaging

dSTORM imaging was performed using a super-resolution PALM/STORM microscope (Roper Scientific, France) customized with a motorized inverted Olympus microscope (IX83). The imaging was carried out using ×100 TIRF/1.49NA at an inclined TIRF angle at the near membrane surface using 647 laser. dSTORM imaging was done as described in Reference 52,53. Under these experimental conditions, the precision of localization for single molecules in dSTORM was between 21 ± 4.3 nm for Alexa 647 as quantified from 2D intensity distributions of 25 isolated single molecules. Sub diffraction limited fiduciary markers of 100 nm diameter (Invitrogen, cat. no. T7279) were used to correct for 2D drift occurring during dSTORM acquisition.[52,53]

2.8 | Image analysis and segmentation: Analysis of nanoscale clusters and shape factors

Clusters of high molecular density (nanodomains) were identified from super-resolution images by a custom algorithm written as a plug-in supported by MetaMorph as described earlier.[53,54] Nanodomains were quantified using bi-dimensional Gaussian fitting, from which the principal (2.3σ long) and the auxiliary axes (2.3σ short, data not shown) were determined.[53–55] The fitting was performed on each cluster that was identified as a domain. The parameters like area and intensity of nanodomain were computed for each category.[53,55] Shape factors for the nanodomain were calculated as the ratio of the minor (axillary axis) to major (principal axis).

The morphometric analysis was also validated with the reference protein PSD95 as reported previously.[53] All experiments and analysis were performed to minimize the errors in quantifying morphology and molecular content of nanodomains.[56,57]

2.9 | Statistical analysis

Graphing and statistical significance was performed using Graph pad prism version 7.04 for windows. All statistical values were shown as Median-IQR (25–75%). Statistical significance was carried out using Mann–Whitney test. Significance was represented by p values described as ***$p < 0.001$ and ****$p < 0.0001$.

3 | RESULTS AND DISCUSSION

3.1 | Dimer-like association of B7-2

The B7-2 IgV domain (residues 0–109, numbering starts after the signaling peptide) was crystallized in the $P2_1$ space group with four molecules in the ASU, named—chains A, B, C, and D (Figure 1a) The structure was refined to R_{work} and R_{free} of 19.9% and 24.8%, respectively, using the data to 1.9 Å. Electron density is continuous for all the residues ranging from 0 to 109 in all the four molecules observed in the ASU. The overall structure is geometrically well defined with 100% residues in the favorable/allowed regions of the Ramachandran plot. A total of 410 residues and 81 molecules of water are present in the ASU. The details of the data and refinement statistics are given in Table 1. All the four molecules in the ASU assume similar antiparallel β-sandwich domain architecture characteristic of the Immunoglobulin superfamily members. The β-sandwich architecture is formed by the antiparallel β sheets, A'BED constituting the back face and the sheets GFCC′ and C″ forming the front face. The front face together with the CC′ and FG-loops of B7-2, harbor residues responsible for binding to CTLA-4.[28] All the four molecules of the ASU are similar to each other

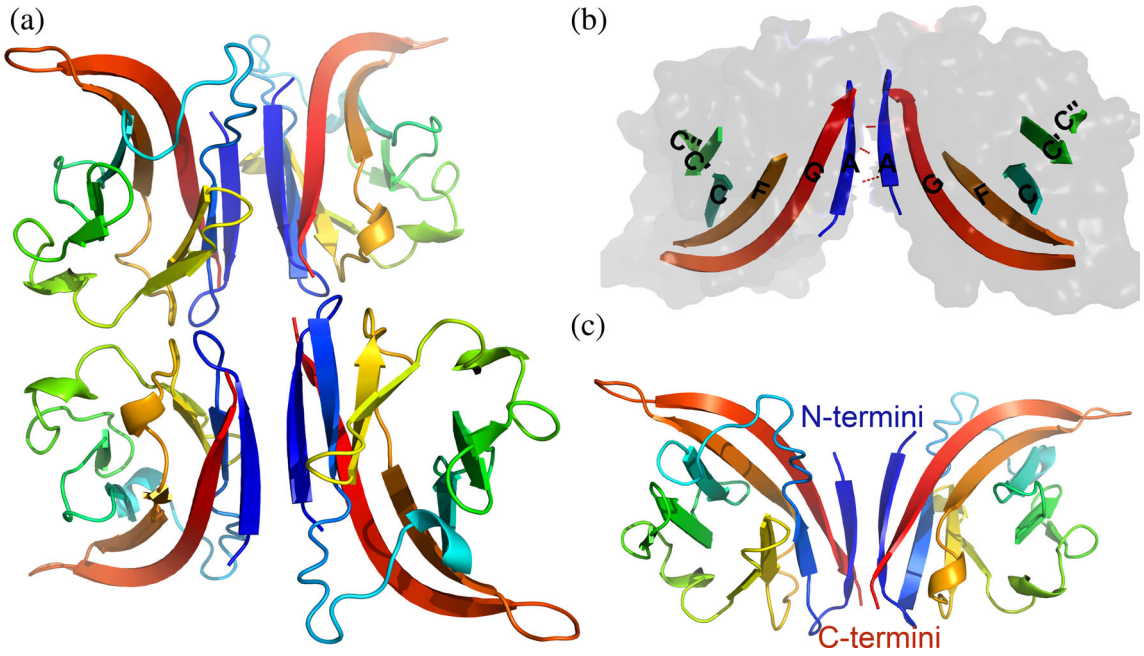

FIGURE 1 (a) Cartoon representation of four B7-2 molecules in the asymmetric unit labelled as chains A, B, C, and D. Chains AB and CD forms two similar dimers. (b) Dimer interface is mediated by three close hydrogen bonds (shown as red dotted lines) between A strands of two protomers of the dimer. The continuous beta sheet formed by the strands A, G, F, C, C′, C″ of both the protomers of the dimer is shown in cartoon representation while the surface view of rest of the molecule is made transparent. (c) Cartoon representation of chain A and chain B is shown in VIBGYOR colours. The N-terminus of both chains is in violet and the C-terminus of both chains is shown in red. Note that the C-terminus of both the associating chains is facing the same direction and are placed close together. The same orientation is maintained with respect to chains C and D in the asymmetric unit

(Figure S1B) with an average RMSD of 0.747 Å as calculated by the program SUPERPOSE (CCP4i).[58] The four molecules in the ASU forms two identical dimer-like associations involving chains AB and CD. Both the dimers are similar to each other with a C_α RMSD of 0.761 Å which is close to RMSD observed between the monomers. The dimer-like interface is formed by three close backbone to backbone hydrogen bonds between N-terminal A strands of both the interacting molecules. Additionally, five potential hydrogen bonds between the protomers of the dimer involving residues Lys2, Gln4, Tyr6, Thr10, and Asp12. Further, such an arrangement results in an extended and highly twisted β-sheet comprising 12 β strands (A, G, F, C, C′ and C″ strands) from the front-face of both protomers involved in the dimer-like association, where each protomer contribute six β strands to the extended β-sheet (Figure 1b). This mode of association brings the C-terminal of the IgV domain (the linking region between the IgV domain and IgC) of two associating molecules close in space separated by a distance of ~18.6 Å (Figure 1c). The interface area buried due to dimerization is around 504 Å^2. Interestingly, this mode of association of membrane distal IgV domains with the C-termini from the associating monomers facing in the same direction appears to be biologically relevant in the context of two monomers emanating from a single cell forming homodimers (*cis*-dimers). To ascertain whether or not this novel dimer-like structure is a result of the altered monomeric structure of the B7-2-IgV domain, we compared the overall structure of the B7-2-IgV domain reported here with the earlier reported structures. The structure of the individual IgV domain is similar to previously determined apo structures of the B72-IgV domain (two molecules in ASU; PDB-entry 1NCN, space group $P2_12_12$) (Figure S1C). Structural comparison revealed that C_α RMSD values vary between a minimum of 0.474 Å and a maximum of 1.074 Å with an average of 0.809 Å. Similarly, these values when compared with B7-2 in the structure of B7-2: CTLA-4 complex (PDB-entry 1I85) had an average C_α RMSD of 1.036 Å, with a maximum deviation of 6.4 Å observed for Thr93 on the FG loop involved in CTLA-4 binding. Despite the similarity in their monomeric structures, the mode of dimer-like association of two B7-2 IgV domains observed in all three structures differs considerably. However, it is interesting to note that the three structures (PDB entries: 1I85, 1NCN, and 5YXK) crystallized in different space groups contain at least one dimer-like orientation with the C-terminus of the

interacting monomers facing in the same direction (Figure S1D[i-iii]).

Whether the dimer-like association observed in our B7-2 structure has any physiological significance or a serendipitous occurrence is a question of interest. Although this kind of dimer-like association is seen for the first time in the case of B7-2, we have found a similar dimer-like association in the case of mouse 2B4 (CD244) (PDB-entry: 2PTU)[59] and human CD58 (PDB entry: 1QA9; chains B and D; Figure 2a–c). Similar to the continuous and fused beta-sheet observed in the B7-2 structure reported here, front-face β-strands of the two associating molecules fuse together to form an extended twisted β-sheet in the above referred two structures too. Further, this mode of association positions the C-terminal ends of both the protomers of the dimer in proximity similar to that observed in our B7-2 dimer-like structure. Similar association has also been observed in many IgV domain-containing structures. For example, five different crystal structures involving TIGIT (apo and complex structures, PDB entries: 3Q0H, 3RQ3, 3UCR, 3UDW, and 5V52) (Figure S3A). In all the cases, the back-face to back-face association is conserved and this association although results in a slightly different relative orientation of protomers of the dimers, involves fusing of β strands of associating protomers to form a single β sheet. Biochemical and cell based experiments confirm that the crystallographically conserved association is important for clustering and signaling through TIGIT/CD226:PVR/nectin-2 axis.[60] A similar edge-edge strand association is observed in four different crystal structures of PD-L1 (PDB entries: 4Z18, 3FN3, 5JDR, 3BIS). Here, in contrast to the other examples, the fusing of β-strands is observed in IgC domain of PD-L1 but not in the IgV domain (Figure S3B). In the example of Axl-Gas6 (Growth arrest-specific gene-6), Axl is a receptor tyrosine kinase which interacts with the ligand-Gas6 and the major interaction surface between them is formed by the β-strands of Axl and Gas6 which align edge-to-edge forming a continuous β-sheet involving both the interacting molecules (Figure S3C).[61] Thus, the fusing of β-strands appears to be a more common mode of association in both homomeric as well as heteromeric interactions. A detailed analysis on the occurrence of fused β-sheets or β-strand interfaces between non-dimeric proteins that form transient oligomers is reported earlier and its physiological significance has been discussed elaborately.[62]

3.2 | Is the observed dimer-like association physiologically relevant?

Analytical ultra-centrifugation, gel filtration and native PAGE analysis suggest B7-2 is a monomer in solution[30,63] and FRET as well as BRET analysis are also suggestive of its monomeric conformation on the membrane.[64,65] In the BRET analysis, B7-2 was used as a standard for monomer together with CD2 with an the assumption that

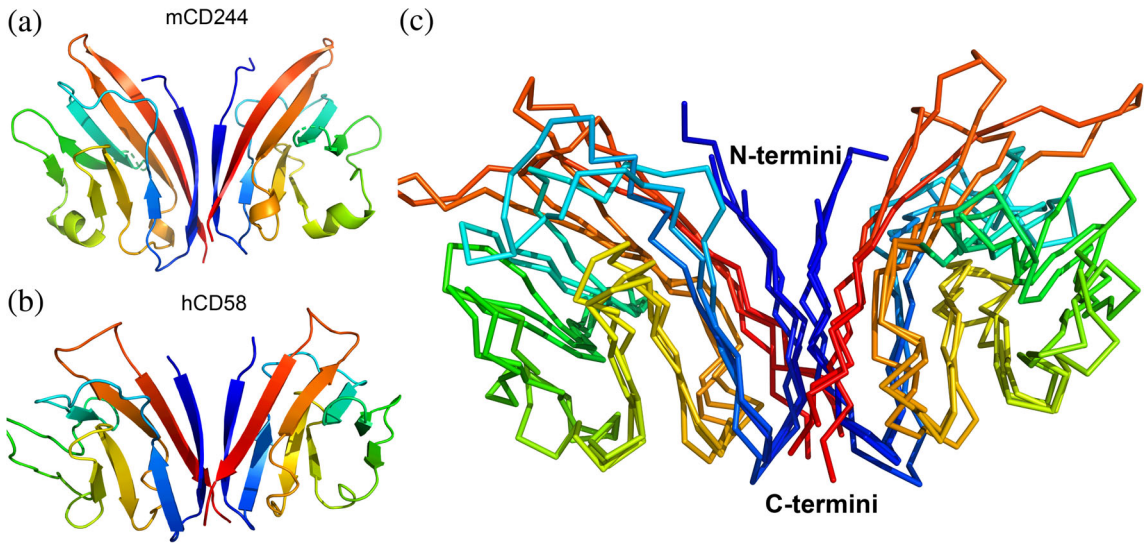

FIGURE 2 Dimer like association observed in hB7-2 structure is similar to that of mouse CD244(2B4) and human CD58 structures. (a) mouse CD244 (PDB entry: 2PTU) structure shown in cartoon representation. (b) human CD58 (PDB entry:1QA9) structure shown in cartoon representation. (c) structures of CD244 and CD58 superposed on B7-2(PDB entry: 5YXK; structure reported in this study) and represented in ribbons. The colours in all the three figures are maintained in VIBGYOR where the N-terminus is shown in violet and the C-terminus is shown in red. Note that all three structures are oriented in a similar fashion and the C-termini of both protomers in all the structures face the same direction in a biologically relevant orientation

the BRETeff maxima observed for B7-2-Luciferase and B7-2-GFP-, BRET-pair represent signal from the monomer. Although B7-2 monomers were observed in the FRET based study. It should be noted that the protein construct used here, however, contains an altered sequence in the EJ-linker part and they propose the possibility of B7-2 oligomerization and clustering at higher concentrations.[64] This situation leads to the question, whether the observed association of B7-2 molecules has any relation to expected oligomerization and clustering[31,64] on the cell surface or in some way helps in the upright orientation of B7-2 molecules on the cell surface or is just an artifact of crystal packing? However, the observed dimer-like association appeared physiologically relevant for the following reasons (1) the front face β-sheets of associating monomers are fused together to form a single twisted β-sheet running through both molecules, which is also observed in the structures of few other important immune receptors (2) assuming such an association is accidental, the probability of repetition of similar dimers in the ASU is infinitesimally small and generally observed only in the case of real dimers. At this stage, we speculated that if this association(*cis*-dimer) is true, it might probably help in the "upright" orientation of B7-2 and hence positions the receptor-binding IgV domain distal to the cell membrane. Since the structure is of only IgV domain, for the observed *cis*-dimer to be relevant, the dimer-like *cis*-association should satisfy the following criteria (1) the IgC domain attached to the *cis*-dimer of IgV domain should be accommodative without any clash or the linker connecting the two domains should be flexible enough to allow large re-arrangements (2) the predicted glycosylation sites should not be the part of the dimeric interface. Since the complete ectodomain structure of B7-2 with IgV and IgC domains is not yet reported, we have employed a systematic study comparing the related structures to answer the above questions.

3.3 | A conserved inter-domain motif of the B7 family

The relative orientation of IgV and IgC domains is expected to have a role in the stability of B7-2 ectodomain, as too much interdomain flexibility could be detrimental to its upright orientation. To this end, we first analyzed the structure of its closest homologue, hB7-1. From this structure (PDB entry: 1DR9), it was clear that the relative orientation of IgV and IgC domains of hB7-1 is constrained by a hydrophobic core formed by the residues Val8, Pro74, Val104, Ala106, Phe134, and Leu163 (Figure 3a). Of these residues, Val8, Pro74, Val104 are part of the IgV domain, and the residues Phe134, Leu163 are from the IgC domain and Ala106 lies on the linker connecting the two domains. The role of the interdomain hydrophobic core on the probable upright orientation of the hB7-1 was speculated in an earlier study.[27] To understand whether this hydrophobic core is also conserved in hB7-2, we modelled the structure of hB7-2 ectodomain (containing both IgC and IgV domains) using the program I-TASSER.

The modelled structure of B7-2 and the crystal structure of B7-1 superposed well with each other (Figure 3a). Although the core structures of the IgC domains are generally similar, the sequence of the B7-2 IgC domain shows low sequence identity with any known IgSF structures, and hence the conformation of the loops varied between different models created by the same program and between different programs used. Similar to hB7-1, a hydrophobic core between IgV and IgC domains consisting of residues Phe8, Ile78, Val108, Ala110, Tyr139, and Leu172 connect the two domains. Hence, although there might be some flexibility, the two domains of B7-2 appear to maintain the relative orientation (Figure 3a). We wondered whether this important structural feature observed in both the human B7 structures is conserved in other species. Sequence analysis of both B7-1 and B7-2, across species with a sequence identity cut-off of min50%–max95% (and with a query coverage of at least 85%) revealed that the inter-domain hydrophobic core is conserved across species in both B7-1 and B7-2 (Figure 3b,c). At this stage, we superposed the modelled B7-2 ectodomain containing both IgV and IgC domain onto individual protomers of the observed β-sheet fused dimer of B7-2 IgV (reported in this study). It was confirmed that the IgC domains thus superposed do not result in any clash (Figure S4), suggesting the front-face fused dimeric association is possible in the presence of the IgC domain. All these observations, together supported the view that the interdomain hydrophobic core indeed has a significant role in the structural integrity of B7-1 and B7-2 proteins and the observed β-sheet fused dimer accommodates the IgC domain without any clash.

To know whether the inter-domain core is a conserved feature in other B7 family members too, multiple sequence alignment of human B7 family members (hB7-1, hB7-2, hB7-H1, hB7-DC, hB7-H2, hB7-H3, hB7-H4, hB7-H6) using Clustal Omega confirmed that the hydrophobic core-forming residues are conserved among all the B7-members (Figure 4a). The sequence alignment also revealed an interesting feature that the inter-domain hydrophobic core contains a conserved -Phe/Tyr-Pro (-F/Y-P)- *cis*-peptide motif in all the B7 family members (Figure 4a,b). Interestingly, despite the low sequence identity among B7 family members, proline

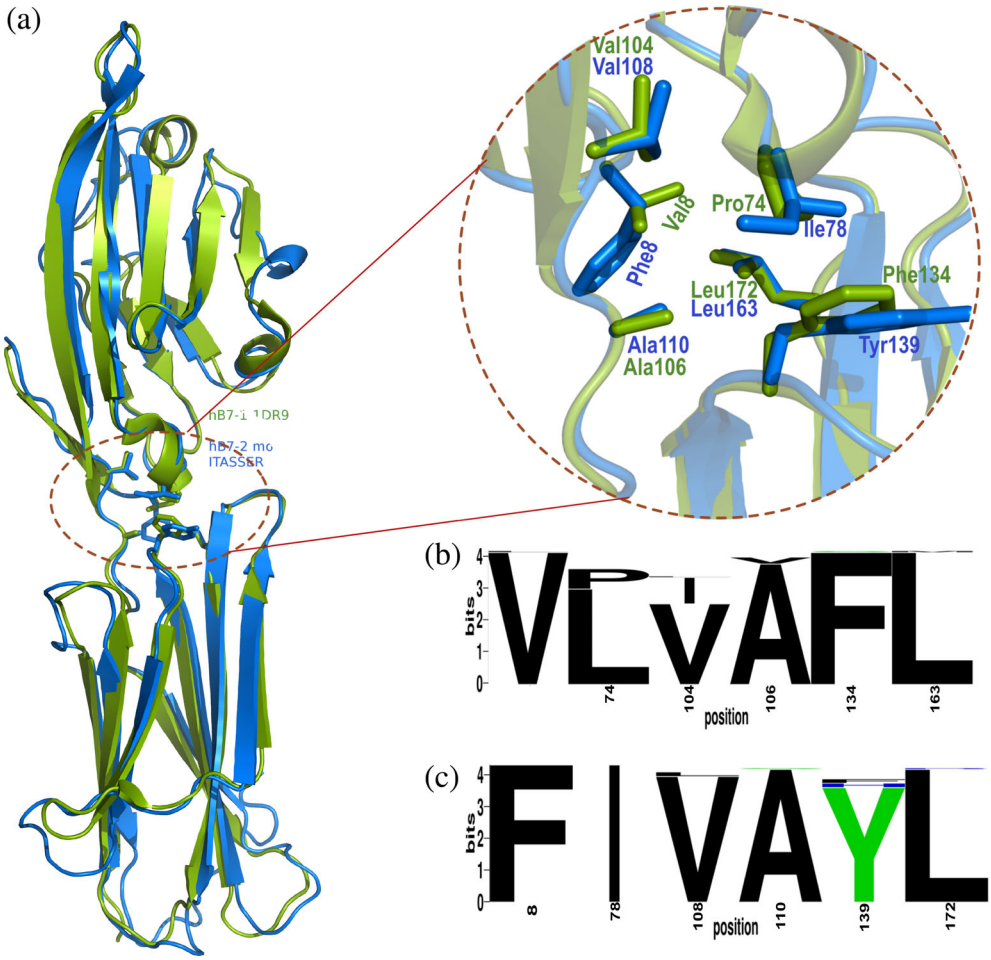

FIGURE 3 Comparison of complete ectodomain structures of hB7-1 (1DR9-green) and hB7-2 modelled with I-TASSER (blue). (a) Ectodomain structure with both IgV and IgC domains of hB7-1 superposed on ectodomain structure of hB7-2 modelled with ITASSER. The superposition reveals over-all similar domain architecture of hB7-1 and hB7-2. The enlarged view of superposed interdomain core of hB7-1 and hB7-2 shows similar hydrophobic interactions in both the structures. (b) Sequence logos representing conserved hydrophobic residues in interdomain core in hB7-1 and (c) in B7-2

involved in the *cis*-peptide is the only residue that is 100% conserved other than the cysteines involved in the canonical disulfide bridge common to the IgSF family (Figure 4b). Also, F and Y together are 100% conserved.

To understand the role of the -F/Y-P- *cis*- peptide motif, we analyzed all the available structures of B7 family members. Our analysis revealed that the aromatic residue (Phe or Tyr) of -F/Y-P- *cis*-peptide motif stacks between the hydrophobic residues of both IgC and IgV domain at the interdomain region and the proline of the *cis* peptide restricts the orientation of the adjacent aromatic residue (F/Y) towards the hydrophobic core (Figure 4c). Thus, -F/Y-P- *cis*-peptide appears to be crucial for maintaining the interdomain hydrophobic core and this core, in turn, might be very crucial in restricting the relative orientation of the two domains in an upright position. Further, hB7-2 contains eight predicted glycosylation sites at positions 8, 22, 110, 121, 129, 152, 167, and 188 (as per Uniprot Id: P42081 and the numbering is based on the sequence devoid of the signal peptide), out of which, two sites are in the IgV domain, five are located in the IgC domain and one site lies in the linker connecting both the domains. Among all the predicted glycosylation sites, only the one at position 8 has been identified at the interface of the observed B7-2 dimer (Figure S4). But close examination of the structure reveals that the sidechain of Asn8 protrudes out of the dimeric interface and the glycan at this position do not hinder the observed dimer-like association.

As mentioned earlier, a 11-residue juxta-membrane linker connects the B7-2 ectodomain with the single-pass transmembrane domain. The flexibility of this linker is also expected to have an impact on the expected "upright" orientation of B7-2 on the cell surface. Interestingly, this linker connecting the IgC domain and the transmembrane domain of B7-2 is rich in conformation constraining proline residues, where a total of five prolines with three in tandem are observed in the sequence (237EDPQPPPDHIP247). This proline-rich sequence suggests that the linker is probably not very flexible. Overall, all the above observations suggest that the ectodomain of B7-2 including the linker is probably rigid enough and hence, even a pliant interaction at the membrane distal IgV domain is sufficient enough to support the "upright" orientation of the complete ectodomain. The front face fused dimer observed here, although weak, is probably capable of providing enough support to keep the B7-2 ectodomain in an erect orientation on the cell surface.

3.4 | B7-2 cluster to form a 1D molecular zipper

Analysis of the crystal-packing leads to another surprise that B7-2 dimers cluster and form 1D nanowire of width around 7 nm (~73 Å) running parallel to crystallographic *a*-axis (Figure 5). The association of both the dimers named AB and CD in the ASU is similar, and each dimer is a part of two distinct 1D arrays that are antiparallel to each other. In this arrangement, the parallel association of dimers creates wedges and groves at the end of the growing 1D nanowire, which is highly complementary to the wedges and groves on the incoming dimer. Further, the C-terminal end of all the molecules in the array are

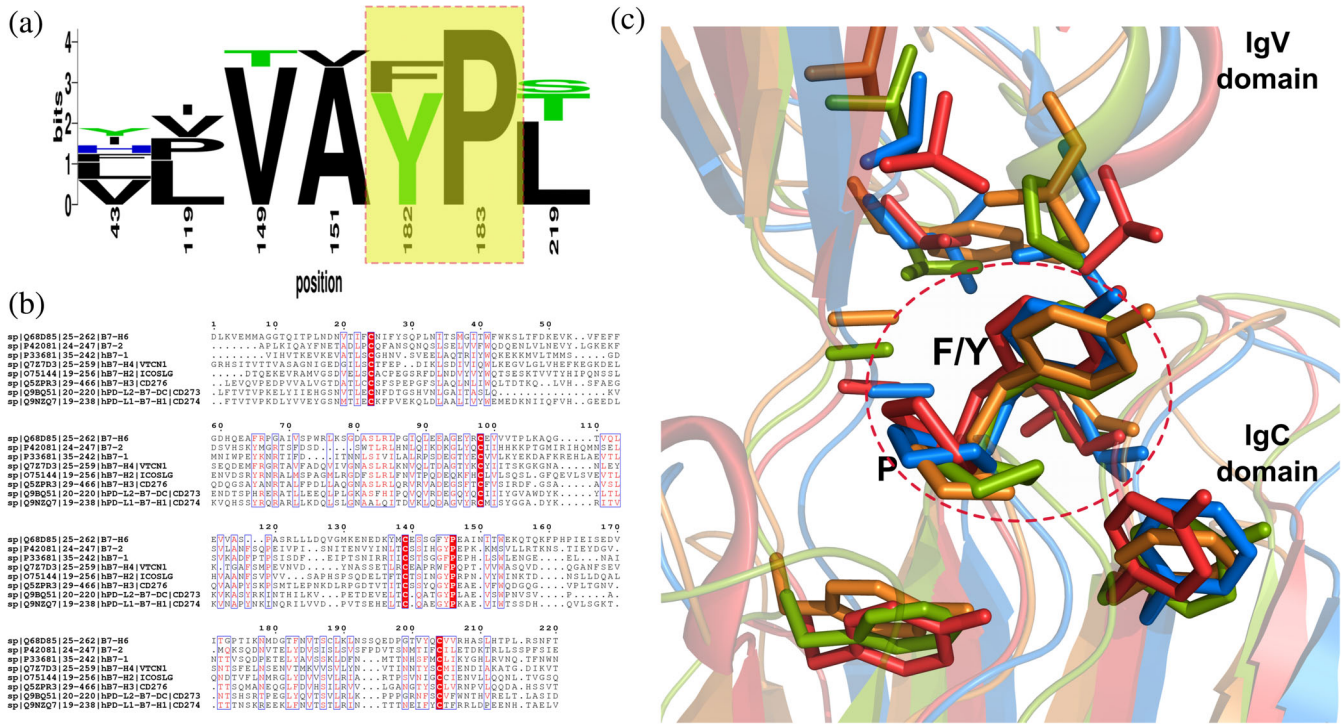

FIGURE 4 F/Y-P cis-peptide in interdomain hydrophobic core is a signature of B7 family members. (a) Sequence logo representing conserved hydrophobic residues in the interdomain core of human B7-family members. The logo was generated from multiple sequence alignment of human B7-family members (hB7-1, hB7-2, hB7-H1, hB7-H2, hB7-H3, hB7-H4, hB7-DC, and hB7-H6). cis-peptide forming proline183 which is 100% conserved and the adjacent aromatic residue F/Y182 are highlighted in rectangular box. (b) MSA of human B7-family members. Note that, despite the over-all similarity among the sequences being very less, the cis-peptide proline is 100% conserved besides the IgSF characteristic canonical disulfide forming cysteines. 100% conserved residues are highlighted in red. (c) Superposition of interdomain hydrophobic core of the available structures of B7-family members—hB7-1 (PDB entry:1DR9; green), hB7-H1(PD-L1; PDB entry: 3BIS; orange), mB7-DC (PD-L2; PDB entry:3BP5; red), and hB7-H6(PDB entry:3PV7; blue). F/Y-P cis peptide is highlighted with a red-dotted circle. Note that the proline of cis-peptide restricts the adjacent aromatic ring to face the hydrophobic core

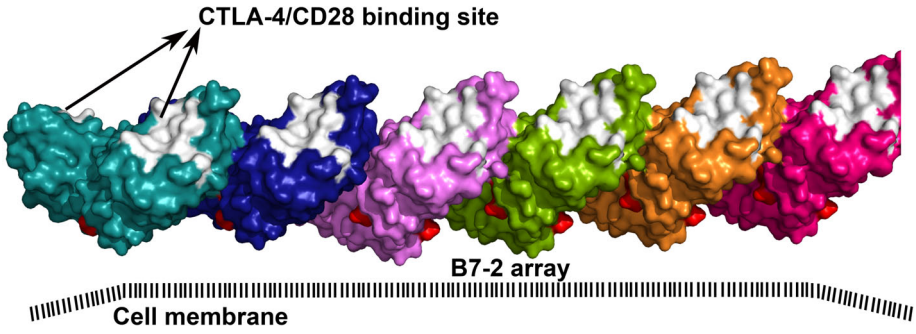

FIGURE 5 B7-2 IgV forms a physiologically relevant 1D molecular zipper in the crystal: one-dimensional zipper like molecular array running parallel to the crystallographic a-axis Note that much of the surface of B7-2 is buried while its CTLA-4/CD28 binding surface, highlighted in light gray, is exposed for all the molecules of the array. The C-termini of all the molecules (shown in red) is facing one direction as if emerging from membrane of a single cell

in the same direction, as if these clustered molecules are emerging from the surface of the same cell. The dimerization of B7-2 and wedge-to-grove arrangement of these dimers in a 1D zipper-like association bury a significant surface area (~1550 Å^2) of each molecule. Consistent with the burial of the significant surface area of each molecule, the observed number of water molecules in the ASU were very less (81 water molecules for 500 residues in ASU). In a 2.0 Å resolution structure, typically the number of water molecules that can be located from the electron density is approximately equal to the number of residues in the ASU, which should have been around 500 water molecules. To understand the orientation and packing of IgC domains in this array, the individual molecules of the complete ectodomain of modeled B7-2 (IgV + IgC) were superposed onto each molecule of the 1D cluster of the IgV domains. It was observed that the IgC domains of each dimer make crisscrossed interactions with the IgC domain of the succeeding and preceding dimers. This way both IgV and IgC domains of each dimer, interact with both preceding and succeeding dimers. However, as mentioned above, the modelling of loops on the IgC domain by any of the programs used (I-TASSER, SWISS-MODEL, Robetta) did not give consistent information on the conformation of the loops probably due to the very low sequence identity of the B7-2 IgC domain with any known structures in wwPDB. Hence, additional studies will be required to determine the complete structure of the ectodomain of B7-2 including juxtamembrane proline-rich sequence to validate our model.

3.5 | Evaluation of B7-2 clustering on the cell surface using super-resolution microscopy

Clustering of B7-2 along with that of MHCII was reported earlier on dendritic cells.[31] To verify whether B7-2 alone forms clusters, we performed dSTORM microscopy on heterologous cell lines expressing B7-2 and counter labeling against the GFP using a combination of anti-GFP antibody and secondary antibody tagged to Alexa647. For comparison, we decided to verify the clustering propensity of both B7-2 and B7-1 on the cell surface. The super-resolved image of B7-2 showed nanoscale compartmentalization of these molecules (Figure S5A–F). A gallery of nanodomains of B7-2 with varying morphology is presented in Figure 6a. Bidimensional gaussian fitting indicated that the larger principal axis of these domains to be 0.16 μm (IQR: 0.10–0.26 μm; Figure 6c). Shape factor was calculated as a ratio of the minor (auxiliary axis) to the major (principal axis) as obtained for the gaussian fitting of nanodomain (Figure 6d). The shape factor for B7-2 was observed as 0.75 (IQR: 0.53–0.89). The intensity of B7-2 in these nanodomains was observed to be 6.61 Gy levels (IQR: 4.56–10.63; Figure 6e). These data indicated that B7-2 is organized into diffraction-limited domains. To verify if this was indeed an organizational signature of B7-2, we collected additional dSTORM images of B7-1 expressing cells, where the protein is known to form stable homodimers. A gallery of nanodomains obtained for B7-1 is presented in (Figure 6b). It was observed that the principal axis of nanodomains of B7-1 was significantly lower than B7-2. The principal axis of B7-1 was 0.11 μm IQR (0.08–0.18 μm) (Figure 6c). Next, we probed the morphology of the nanodomain for B7-1 by evaluating the shape factors. The distribution of the shape factors confirmed that nanodomains of B7-2 were more ellipsoidal than the nanodomains of B7-1 (0.84, IQR: 0.63–0.93) (Figure 6d). This indicates that the inherent clustering of B7-2 and B7-1 are different, and elongated or ellipsoidal organization is observed for B7-2. We then evaluated if there are any differences in the density of molecules in the nanodomains. We extracted cluster intensity for each condition. We found that in the case of B7-1 (6.49; IQR 4.61–9.56; Figure 6e), the cluster intensity was reduced in comparison to B7-2.

3.6 | Is the cluster functionally relevant?

We pondered, whether the CTLA-4 or the CD28 from the opposing cell can access the binding site on B7-2 involved in clustering? The key interacting residues of the CTLA-4 and the CD28 are located on the FG loop, which is identical (sequence: -MYPPPY-) between the two proteins. The binding site for CD28/CTLA-4 on B7-2 has already been defined based on the mutational studies.[66] Further, the crystal structure of the CTLA-4:B7-2 complex also gives a detailed information on their binding interface,[28] although no structural details of the CD28: B7-2 complex are available. As mentioned before, in the 1D array, the major part of the exposed surface on B7-2 is the binding surface of CTLA-4/CD28. Also, the exposed binding site is carved out of the CC′ loop, the front-face and the FG-loop of B7-2 IgV domain and this binding site is located on both sides of the array (Figure 5). Further, from the crystal structures of apo and CTLA-4 bound B7-2, it can be observed that the FG-loop undergoes a slight conformational change of ~6.4 Å upon CTLA-4 binding. Consistent with this observation, the FG-loop of B7-2 is a part of the exposed surface and is free to accommodate conformational changes required for CTLA-4 binding. Furthermore, superposition of B7-2 from B7-2:CTLA-4 structure containing an individual molecule of B7-2 and CTLA-4 (PDB entry: 1I85) on to the individual domains

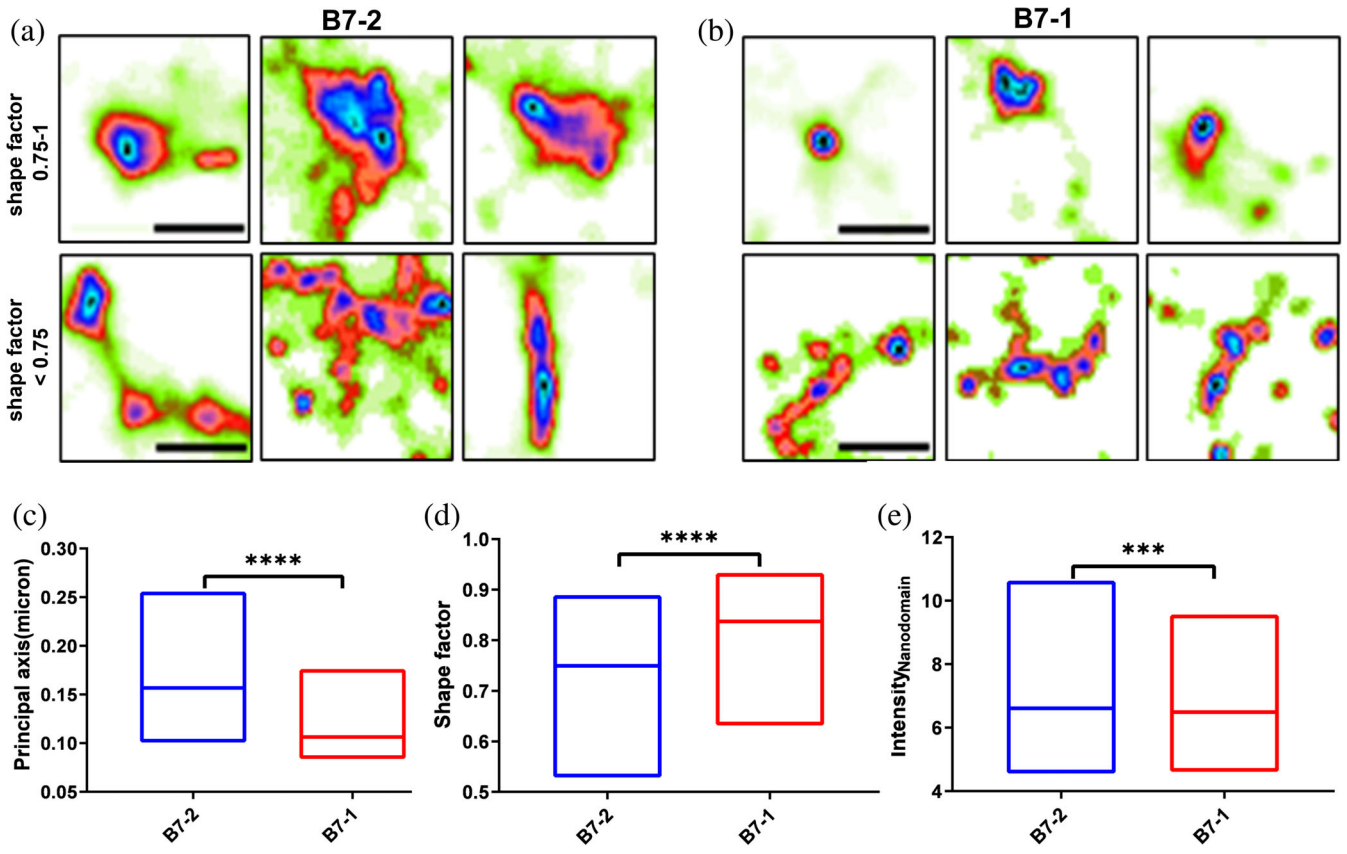

FIGURE 6 Super-resolution microscopy to observe clustering of B7-2: A and B represents the gallery of nanodomains for B7-2 and B7-1, respectively. Top panel represents the nanodomains having shape factor 0.75 to 1 and the panel below represents the nanodomains having shape factor <0.75. C, D, and E indicate the principal axis, shape factor and average intensity for the nanodomains of B7-2 and B7-1, respectively. $n = 4{,}661$ nanodomains for B7-2 and $n = 9918$ nanodomains for B7-1. Data points represent interquartile range-Median (IQR25% to 75%). Statistical test is Mann–Whitney test; ***$p < 0.001$ and ****$p < 0.0001$. Scale bar at A and B is 0.5 μm

of observed B7-2 array, positions the monomeric CTLA-4 molecules without any clash. Moreover, this arrangement of B7-2 and CTLA-4 places their C-termini in opposite direction that is appropriate for CTLA-4 molecules from the juxtaposed cell (Figure S6A). The above observations collectively assert the physiological relevance of observed B7-2 clustering.

As mentioned before, the dimer-like association of B7-2 in our structure resembles that of human CD58 (in hCD2-hCD58 complex, PDB entry: 1QA9). hCD2 expressed on T-cells and NK cells makes heterophilic interaction with hCD58 (LFA-3) expressed on APCs.[67] Both CD2 and CD58 belong to the subset of IgSF and mediate the adhesion of T-cell and APC. Moreover, they are shown to be part of cSMAC where CD28: B7 molecules are also clustered at the IS.[15] Surprisingly, in the CD58:CD2 complex, CD58 forms 1D zipper-like array similar to what we observed in our B7-2 structure. Further, while most of the surface of CD58 is buried in the array, the CD2 binding site located on either side of the array is exposed (similar to the CTLA-4 binding site on the B7-2 array). In fact, the superposition of one of the dimers of the B7-2 array onto the CD58 dimer of the CD58 array superposes the complete array with each other. Also, in the hCD2:hCD58 structure (PDB entry: 1QA9), CD2 binds along and on both sides of the CD58 array as if the two partners approach from juxtaposed cells (Figure S6B). This might also explain the conundrum of a high 2D affinity exhibited by these molecules on cell surface despite their low affinity and faster dissociation rates.[68–70] It appears to be inevitable for constitutively expressed molecules like B7-2, to have an efficient mechanism that avoids spurious signaling. In the case of T-cell receptors (TCR) and Lat, it has been proposed that clustering and spatial segregation of these receptors have a role in the avoidance of spurious ZAP-70 activation.[33] Similarly, if the self-clustering of B7-2 is also designed to avoid spurious signaling, then, the architecture of such a cluster should hinder unintended association of CD28/CTLA-4 dimer with B7-2 on the opposing cell and consequent signaling. On the other hand, this clustering should not completely bury the CTLA-4/CD28 binding

surface on B7-2 making its interaction with the receptors difficult. Superposition of B7-2 from CTLA-4:B7-2 complex (in this case with a CTLA-4 dimer, PDB entry:1I85) on to a B7-2 monomer on the array suggests that when one molecule of the CTLA-4 dimer binds B7-2, the second protomer of the CTLA-4 dimer is positioned away from the array without any interaction with the array (Figure S7A). The observation is consistent with the expected behavior, as the mode of B7-2 dimerization in the pre-existing array observed here should be different from that of receptor-induced dimeric B7-2 array which has an alternate 1D arrangement of induced B7-2 dimers and CTLA-4 dimers. Then the question remains, how the pre-existing B7-2 1D array or cluster rearrange to form induced dimer?

During the activation phase of the T-cell, the expression of cognate partners of B7-2 are upregulated on the T-cell and are abundantly available at IS. To mimic this situation, we engaged all the B7-2 molecules of the 1D array with the CTLA-4 dimer to verify whether the pre-existing cluster can accommodate the over-expressed receptors. It was interesting to observe that the second protomer of each CTLA-4 dimer (which is not interacting with B7-2 on the array) makes steric clash with adjacent CTLA-4 molecules, suggesting this array cannot accommodate two dimers adjacent to each other on the array (Figure S7A). Probably, the strain exerted on the weak B7-2 assembly due to successive association of strong disulfide-linked CTLA-4 dimers on to B7-2 results in dissociation of the pre-existing B7-2 assembly. This paves way for its rearrangement into alternate B7-2 and CTLA-4 dimers resulting in a 1D lattice as observed in the crystal structure of CTLA-4:B7-2 complex (Figure S7B) that is proposed to represent postsynaptic situation. This way, the observed B7-2 clustering probably avoids spurious signaling despite its constitutive expression, and only sufficient expression and concentration of dimeric cognate receptors (CTLA-4/CD28) can dissociate the pre-signaling cluster of B7-2 and induce signaling.

4 | CONCLUSION

Compartmentalization of receptors on the membrane and their dynamics are the key regulators of cell signaling. Despite its importance, the exact nature of these clusters and the underlying principles that govern the organization of these cell surface proteins are not clear. The B7-2 array presented here appears to provide important insights on the signaling through CTLA-4:B7-2 axis. First, it provides insight regarding how monomeric proteins like B7-2 stand upright on the cell surface keeping their IgV domains (that interacts with the receptors) distal to the membrane. Second, such inherent self-association into an array is the probable reason for the observed B7-2 clustering on the cell surface, where 1D arrays can stack adjacent to each other on the cell-surface forming clusters of different architecture and size. Thirdly, the array appears to provide an explanation for the avoidance of spurious signaling and rearrangement into a receptor-induced dimer in the presence of sufficient expression of CTLA-4 dimers on the juxtaposed T-cell. Although, super-resolution microscopy experiments suggest that B7-2 clusters are relatively larger and elongated compared to B7-1 cluster, we could not resolve the association preference of these molecules on the cell surface. Unfortunately, we lack the tools and techniques to observe such an array with a width close to 7 nm (super-resolution microscopy, which is proposed to supersede its theoretical limit of 200 nm can only reach around 10–20 nm). We believe, in the future, electron-tomography or other similar techniques will resolve the mysteries related to compartmentalization and clustering of these signaling receptors.

ACKNOWLEDGMENTS

Udupi A. Ramagopal would like to thank Vision Group on Science and Technology (VGST), grant #191, Karnataka, India. Swetha Lankipalli would like to acknowledge the fellowship from CSIR (2013–2018), Government of India and Bristol Myers Squibb (from 2019). Udupi A. Ramagopal and Swetha Lankipalli would like to acknowledge Admar Mutt Education Foundation (AMEF) for the support and ESRF-Grenoble synchrotron radiation facility-DBT India collaboration for data collection. We also thank Prof. Ranga Udayakumar, JNCASR, Bangalore for his support. Deepak Nair thank Dr Jean-Baptiste Sibarita, IINS, Bordeaux, France, for sharing of analysis tools used in the manuscript and grants of DBT-IISc Partnership Program (D.N), IISC-STARs program grant (D.N; PID 563), Indian Institute of Science (Institute of Excellence Program) for generous support.

CONFLICT OF INTEREST

The authors declare no conflict of interest.

AUTHOR CONTRIBUTIONS

Swetha Lankipalli: Conceptualization; data curation; formal analysis; investigation; methodology; writing-original draft; writing-review & editing. **Mahadeva Swamy H S:** Data curation; formal analysis; investigation; methodology; writing-original draft. **Deepak Selvam:** Formal analysis; investigation; methodology; writing-review & editing. **Dibyendu Samanta:** Investigation; methodology; resources; supervision; writing-review & editing. **Deepak Nair:** Formal analysis;

methodology; resources; software; supervision; validation; writing-original draft; writing-review & editing. **Udupi Ramagopal:** Conceptualization; data curation; formal analysis; funding acquisition; investigation; methodology; project administration; resources; software; supervision; validation; visualization; writing-original draft; writing-review & editing.

DATA AVAILABILITY STATEMENT

The diffraction and structural data have been submitted to protein data bank with PDB-entry 5YXK and authors agree to make all protocols and data available for the readers.

ORCID

Dibyendu Samanta https://orcid.org/0000-0002-5733-6694
Deepak Nair https://orcid.org/0000-0002-2103-1653
Udupi A. Ramagopal https://orcid.org/0000-0003-1045-9838

REFERENCES

1. Greenwald RJ, Freeman GJ, Sharpe AH. The B7 family revisited. Annu Rev Immunol. 2005;23:515–548.
2. Lafferty KJ, Cunningham AJ. A new analysis of allogeneic interactions. Aust J Exp Biol Med Sci. 1975;53:27–42.
3. Babcock SK, Gill RG, Bellgrau D, Lafferty KJ. Studies on the two-signal model for T cell activation in vivo. Transplant Proc. 1987;19:303–306.
4. Carreno BM, Collins M. The B7 family of ligands and its receptors: New pathways for costimulation and inhibition of immune responses. Annu Rev Immunol. 2002;20:29–53.
5. Grakoui A, Bromley SK, Sumen C, et al. The immunological synapse: A molecular machine controlling T cell activation. Science. 1999;285:221–227.
6. Alarcon B, Mestre D, Martinez-Martin N. The immunological synapse: A cause or consequence of T-cell receptor triggering? Immunology. 2011;133:420–425.
7. Monks CR, Freiberg BA, Kupfer H, Sciaky N, Kupfer A. Three-dimensional segregation of supramolecular activation clusters in T cells. Nature. 1998;395:82–86.
8. Linsley PS, Brady W, Grosmaire L, Aruffo A, Damle NK, Ledbetter JA. Binding of the B cell activation antigen B7 to CD28 costimulates T cell proliferation and interleukin 2 mRNA accumulation. J Exp Med. 1991;173:721–730.
9. Walunas TL, Lenschow DJ, Bakker CY, et al. CTLA-4 can function as a negative regulator of T cell activation. Immunity. 1994;1:405–413.
10. Tivol EA, Borriello F, Schweitzer AN, Lynch WP, Bluestone JA, Sharpe AH. Loss of CTLA-4 leads to massive lymphoproliferation and fatal multiorgan tissue destruction, revealing a critical negative regulatory role of CTLA-4. Immunity. 1995;3:541–547.
11. Borriello F, Sethna MP, Boyd SD, et al. B7-1 and B7-2 have overlapping, critical roles in immunoglobulin class switching and germinal center formation. Immunity. 1997;6:303–313.
12. Collins M, Ling V, Carreno BM. The B7 family of immune-regulatory ligands. Genome Biol. 2005;6:223.
13. van der Merwe PA, Davis SJ. Molecular interactions mediating T cell antigen recognition. Annu Rev Immunol. 2003;21:659–684.
14. Pentcheva-Hoang T, Egen JG, Wojnoonski K, Allison JP. B7-1 and B7-2 selectively recruit CTLA-4 and CD28 to the immunological synapse. Immunity. 2004;21:401–413.
15. Dustin ML, Chakraborty AK, Shaw AS. Understanding the structure and function of the immunological synapse. Cold Spring Harb Perspect Biol. 2010;2:a002311.
16. Vincenti F, Dritselis A, Kirkpatrick P. Belatacept. Nat Rev Drug Discov. 2011;10:655–656.
17. Massarotti EM. Clinical and patient-reported outcomes in clinical trials of abatacept in the treatment of rheumatoid arthritis. Clin Ther. 2008;30:429–442.
18. Fellner C. Ipilimumab (yervoy) prolongs survival in advanced melanoma: Serious side effects and a hefty price tag may limit its use. P T. 2012;37:503–530.
19. Chen CL, Huang J, Wang, CH. et al. Hepatitis C virus has a genetically determined lymphotropism through co-receptor B7.2. Nat Commun. 2017;8:13882.
20. Bounou S, Dumais N, Tremblay MJ. Attachment of human immunodeficiency virus-1 (HIV-1) particles bearing host-encoded B7-2 proteins leads to nuclear factor-kappa B- and nuclear factor of activated T cells-dependent activation of HIV-1 long terminal repeat transcription. J Biol Chem. 2001;276:6359–6369.
21. Short JJ, Vasu C, Holterman MJ, Curiel DT, Pereboev A. Members of adenovirus species B utilize CD80 and CD86 as cellular attachment receptors. Virus Res. 2006;122:144–153.
22. Xu Z, Shen J, Wang, MH. et al. Comprehensive molecular profiling of the B7 family of immune-regulatory ligands in breast cancer. Onco Targets Ther. 2016;5:e1207841. https://doi.org/10.1080/2162402X.2016.1207841.
23. Anne Florcken MJ, Nguyen-Hoai T, Gerhardt A, et al. Immunomodulatory molecules in renal cell cancer: CD80 and CD86 are expressed on tumor cells. Intl J Clin Exper Pathol. 2017;10:11.
24. Ni L, Dong C. New B7 family checkpoints in human cancers. Mol Cancer Ther. 2017;16:1203–1211.
25. Freeman GJ, Gribben J, Boussiotis V, et al. Cloning of B7-2: A CTLA-4 counter-receptor that costimulates human T cell proliferation. Science. 1993;262:909–911.
26. Stamper CC, Zhang Y, Tobin JF, et al. Crystal structure of the B7-1/CTLA-4 complex that inhibits human immune responses. Nature. 2001;410:608–611.
27. Ikemizu S, Gilbert RJC, Fennelly JA, et al. Structure and dimerization of a soluble form of B7-1. Immunity. 2000;12:51–60.
28. Schwartz JC, Zhang X, Fedorov AA, Nathenson SG, Almo, SC. Structural basis for co-stimulation by the human CTLA-4/B7-2 complex. Nature. 2001;410:604–608.
29. Zhang X, Schwartz JCD, Almo SC, Nathenson SG. Crystal structure of the receptor-binding domain of human B7-2: Insights into organization and signaling. Proc Natl Acad Sci USA. 2003;100:2586–2591.
30. Zhang X, Schwartz JCD, Almo SC, Nathenson SG. Expression, refolding, purification, molecular characterization,

crystallization, and preliminary X-ray analysis of the receptor binding domain of human B7-2. Protein Expr Purif. 2002;25:105–113.
31. Turley SJ, Inaba K, Garrett WS, et al. Transport of peptide-MHC class II complexes in developing dendritic cells. Science. 2000;288:522–527.
32. Greene JL, Leytze GM, Emswiler, J. et al. Covalent dimerization of CD28/CTLA-4 and oligomerization of CD80/CD86 regulate T cell costimulatory interactions. J Biol Chem. 1996;271:26762–26771.
33. Chung W, Abel SM, Chakraborty AK. Protein clusters on the T cell surface may suppress spurious early signaling events. PLoS One. 2012;7:e44444.
34. Garcia-Parajo MF, Cambi A, Torreno-Pina JA, Thompson N, Jacobson K. Nanoclustering as a dominant feature of plasma membrane organization. J Cell Sci. 2014;127:4995–5005.
35. Simons K, Ikonen E. Functional rafts in cell membranes. Nature. 1997;387:569–572.
36. Gowrishankar K, Ghosh S, Saha S, C. R, Mayor S, Rao M. Active remodeling of cortical Actin regulates spatiotemporal organization of cell surface molecules. Cell. 2012;149:1353–1367.
37. Kotani N, Gu J, Isaji T, Udaka K, Taniguchi N, Honke K. Biochemical visualization of cell surface molecular clustering in living cells. Proc Natl Acad Sci USA. 2008;105:7405–7409.
38. Honig B, Shapiro L. Adhesion protein structure, molecular affinities, and principles of cell-cell recognition. Cell. 2020;181:520–535.
39. Lankipalli S, Ramagopal UA. How does an ectodomain of membrane-associated proteins stand upright and exert robust signal? bioRxiv. 2021;2020.07.29.226837.
40. Harrison OJ, Jin X, Hong S, et al. The extracellular architecture of adherens junctions revealed by crystal structures of type I cadherins. Structure. 2011;19:244–256.
41. Aslanidis C, de Jong PF. Ligation-independent cloning of PCR products (LIC-PCR). Nucleic Acids Res. 1990;18:6069–6074.
42. Minor W, Cymborowski M, Otwinowski Z, Chruszcz M. HKL-3000: The integration of data reduction and structure solution—from diffraction images to an initial model in minutes. Acta Cryst D. 2006;62:859–866.
43. Vagin A, Teplyakov A. Molecular replacement with MOLREP. Acta Cryst D. 2010;66:22–25.
44. Murshudov GN, Skubák P, Lebedev AA, et al. REFMAC5 for the refinement of macromolecular crystal structures. Acta Cryst D. 2011;67:355–367.
45. Emsley P, Lohkamp B, Scott WG, Cowtan K. Features and development of Coot. Acta Cryst D. 2010;66:486–501.
46. Altschul SF, Gish W, Miller W, Myers EW, Lipman DJ. Basic local alignment search tool. J Mol Biol. 1990;215:403–410.
47. McWilliam H, Li W, Uludag M, et al. Analysis tool web services from the EMBL-EBI. Nucleic Acids Res. 2013;41:W597–W600.
48. Robert X, Gouet P. Deciphering key features in protein structures with the new ENDscript server. Nucleic Acids Res. 2014;42:W320–W324.
49. Olsen LR, Kudahl UJ, Simon, C. et al. BlockLogo: visualization of peptide and sequence motif conservation. J Immunol Methods. 2013;400–401:37–44.
50. Venkatachalapathy M, Belapurkar V, Jose M, Gautier A, Nair D. Live cell super resolution imaging by radial fluctuations using fluorogen binding tags. Nanoscale. 2019;11:3626–3632.
51. Tanwar M, Kateriya S, Nair D, Jose M. Optogenetic modulation of real-time nanoscale dynamics of HCN channels using photoactivated adenylyl cyclases. RSC Chem Biol. 2021;2:863–875.
52. Nanguneri S, Pramod RT, Nadia, E. et al. Characterization of nanoscale organization of F-actin in morphologically distinct dendritic spines in vitro using supervised learning. eNeuro. 2019;6:ENEURO.0425-18.2019. https://doi.org/10.1523/ENEURO.0425-18.2019.
53. Kedia S, Ramakrishna P, Netrakanti PR, et al. Real-time nanoscale organization of amyloid precursor protein. Nanoscale. 2020;12:8200–8215.
54. Nair D, Hosy E, Petersen JD, et al. Super-resolution imaging reveals that AMPA receptors inside synapses are dynamically organized in nanodomains regulated by PSD95. J Neurosci. 2013;33:13204–13224.
55. Kedia S, Ramakrishna P, Netrakanti, PR. et al. Alteration in synaptic nanoscale organization dictates amyloidogenic processing in Alzheimer's disease. iScience. 2021;24:101924. https://doi.org/10.1016/j.isci.2020.101924.
56. Khater IM, Nabi IR, Hamarneh G. A review of super-resolution single-molecule localization microscopy cluster analysis and quantification methods. Patterns. 2020;1:100038.
57. Baumgart F, Arnold AM, Leskovar K, et al. Varying label density allows artifact-free analysis of membrane-protein nanoclusters. Nat Methods. 2016;13:661–664.
58. Collaborative Computational Project N. The CCP4 suite: Programs for protein crystallography. Acta Cryst D. 1994;50:760–763.
59. Velikovsky CA, Deng L, Chlewicki LK, Fernández MM, Kumar V, Mariuzza RA. Structure of natural killer receptor 2B4 bound to CD48 reveals basis for heterophilic recognition in signaling lymphocyte activation molecule family. Immunity. 2007;27:572–584.
60. Stengel KF, Harden-Bowles K, Yu X, et al. Structure of TIGIT immunoreceptor bound to poliovirus receptor reveals a cell-cell adhesion and signaling mechanism that requires cis-trans receptor clustering. Proc Natl Acad Sci USA. 2012;109:5399–5404.
61. Sasaki T, Knyazev PG, Clout NJ, et al. Structural basis for Gas6-Axl signalling. EMBO J. 2006;25:80–87.
62. Feverati G, Achoch M, Zrimi J, Vuillon L, Lesieur C. Beta-strand interfaces of non-dimeric protein oligomers are characterized by scattered charged residue patterns. PLoS One. 2012;7:e32558.
63. Collins AV, Brodie DW, Gilbert RJC, et al. The interaction properties of costimulatory molecules revisited. Immunity. 2002;17:201–210.
64. Bhatia S, Edidin M, Almo SC, Nathenson SG. Different cell surface oligomeric states of B7-1 and B7-2: Implications for signaling. Proc Natl Acad Sci USA. 2005;102:15569–15574.
65. James JR, Oliveira MI, Carmo AM, Iaboni A, Davis SJ. A rigorous experimental framework for detecting protein oligomerization using bioluminescence resonance energy transfer. Nat Methods. 2006;3:1001–1006.
66. Peach RJ, Bajorath J, Naemura J, et al. Both extracellular immunoglobin-like domains of CD80 contain residues critical for binding T cell surface receptors CTLA-4 and CD28. J Biol Chem. 1995;270:21181–21187.

67. Selvaraj P, Plunkett ML, Dustin M, Sanders ME, Shaw S, Springer TA. The T lymphocyte glycoprotein CD2 binds the cell surface ligand LFA-3. Nature. 1987;326:400–403.
68. Dustin ML, Golan DE, Zhu DM, et al. Low affinity interaction of human or rat T cell adhesion molecule CD2 with its ligand aligns adhering membranes to achieve high physiological affinity. J Biol Chem. 1997;272:30889–30898.
69. van der Merwe PA, Barclay AN, Mason DW, et al. Human cell-adhesion molecule CD2 binds CD58 (LFA-3) with a very low affinity and an extremely fast dissociation rate but does not bind CD48 or CD59. Biochemistry. 1994;33:10149–10160.
70. Bromley SK, Iaboni A, Davis SJ, et al. The immunological synapse and CD28-CD80 interactions. Nat Immunol. 2001;2:1159–1166.

SUPPORTING INFORMATION

Additional supporting information may be found online in the Supporting Information section at the end of this article.

How to cite this article: Lankipalli S, H S MS, Selvam D, Samanta D, Nair D, Ramagopal UA. Cryptic association of B7-2 molecules and its implication for clustering. Protein Science. 2021;30:1958–1973. https://doi.org/10.1002/pro.4151